Nuclear magnetic resonance force microscopy at millikelvin temperatures

Haan, A.M.J. den

Chapter 3

Theory and experimental improvements

Improving the sensitivity of an MRFM system to enable fast measurements of single nuclear spins opens paths to new imaging methods of biological samples and condensed matter research. However, improving this sensitivity is one of the difficulties in MRFM. In this chapter we will discuss the limiting factors and requirements for a successful MRFM experiment.
In section 3.1, we discuss the main noise source and the resulting sensitivity. Since many of the experiments are performed by measuring a frequency shift, we discuss in section 3.2 the noise present in these frequency measurements. Then in section 3.3, we compare the signal to noise ratio for a force measurement and a frequency measurement. In section 3.4, we discuss the requirement of the spin lattice relaxation time (T_1 time) of spins, which needs to be in a certain range in order to measure it. Another more technical requirement is to reduce the heat which is produced when applying a B_1 field. This will be described in section 3.5. Finally, in section 3.6 the issue of repulsion between the magnetic particle and the superconducting structures will be discussed.

3.1 Sensitivity and force noise

Thermal force noise is one of the fundamental noise sources limiting the sensitivity of MRFM. In chapter 2, we already introduced the thermal force noise (Eq. 2.9). One has to minimize this force noise noise in order to increase the force sensitivity. As mentioned in section 2.1, one of our strategies is to lower the temperature to millikelvin temperatures. The other factor is the damping $\Gamma = \frac{\sqrt{km}}{Q}$, which sets the design parameters for the cantilever. For a rectangular cantilever, the damping is given by:

$$\Gamma = \frac{\sqrt{E}\rho w t^2}{QL} \tag{3.1}$$

Where we used $k_0 = \frac{Ewt^3}{4L^3}$, in which E is the Young's modulus, ρ is the density of the material and w, t, and L are the width, thickness and length of the cantilever respectively. From this equation, one could argue that a long, very thin and narrow cantilever with low density material leads to low damping. However, the Quality factor Q can vary with each of these parameters (dimensions, Young's modulus and material). The main dissipation channels are via impurities, defects, surface dissipation, and clamping losses [32, 33, 34]. Significant effort has been undertaken to improve on these properties [16, 35, 36, 37, 24]. When surface dissipation is dominant, we can assume that Quality factor is linearly dependent on the thickness, as can be seen in reference [16]. In this case, a specific mechanical dissipation factor α can be defined, which is independent of geometry [16]:

$$\alpha = \frac{\sqrt{E\rho}}{Q/t} \tag{3.2}$$

Hence,

$$\Gamma = \frac{\alpha w t}{L} \tag{3.3}$$

It then follows that the damping is still lowered by decreasing the width and thickness, and increasing the length.

If we compare the force noise Eq. 2.9 to the minimum detectable force from a single spin: $F_{min} = G\mu_{min}$, we see that the minimum magnetic moment which can be detected is [19]:

$$\mu_{min} = \frac{1}{G}\sqrt{4\Gamma k_B T \Delta f} \tag{3.4}$$

Where $G = \frac{\partial B}{\partial x}$ is the gradient field. From this equation we see that the size of the particle is an important factor, since the gradient field is inversely proportional to the distance (r) to the fourth power $G \propto r^{-4}$. Therefore it is useful to put effort into downsizing the magnetic particle. In chapter 4, the fabrication of a micron sized high gradient magnet will be discussed.

For typical values of the cantilever as shown in figure 2.4 in our cryostat, with eigenfrequency $f_0 = 3$ kHz, quality factor $Q = 10000$, and a spring constant $k_0 = 8 \cdot 10^{-}5$, the spectral density of the force noise is: $S_F = 1\,\mathrm{aN}/\sqrt{\mathrm{Hz}}$ at a temperature of 50 mK. For a gradient field of 10^5T/m (for a 3 μm diameter NdFeB magnet of remanent magnetization $\mu_0 M = 1.3T$ at 1 μm distance from the surface) and using the typical values for the MRFM cantilever, the minimum magnetic moment in a 1 Hz bandwidth is $\frac{1\,\mathrm{aN}}{10^5\,\mathrm{T/m}} = 1 \cdot 10^{-23}$ J/T. This is in the order of 1 electron spin or 100 nuclear spins.

Recent development of low dissipation in cantilevers has resulted in diamond cantilevers with a quality factor of 6 Million at 100 mK [16]. With an optimized cantilever of this type, it is possible to obtain a force noise sensitivity of $45\,\mathrm{zN}/\sqrt{\mathrm{Hz}}$ at 100 mK. Assuming that no dissipative noise is present from the sample, this force noise sensitivity enables measurements of single nuclear spins in a measurement time of one second with a gradient field of $1 \cdot 10^6$T/m. The minimum magnetic moment is in this case $4.5 \cdot 10^{-26}$J/T.

3.2 Frequency noise

Frequency modulation of a cantilever is widely used in atomic force microscopy to measure spring constant changes due to gradient forces on the cantilever [38, 39]. In MRFM we use the same technique to measure the interaction of the nuclear spins on the MRFM cantilever. Frequency shift is measured due to reorientation of nuclear spins which change the gradient force. The method of using frequency shift is used in many MRFM experiments, such as in Cantilever Enabled Readout of Magnetization Inversion Transients (CERMIT) and saturation experiments [40, 41].

In chapter 7, a saturation experiment on copper is described in detail for which frequency shifts are used to detect spins in copper. In this section we will provide a basic description of the noise present in a frequency shift measurement. In many cases, the frequency shift is measured by using a phase locked loop, which keeps track of the cantilever frequency by keeping the phase at a fixed value by means of a PID controller and a voltage controlled oscillator. Another way is to self-oscillate the cantilever at its resonance frequency in which the cantilever is driven by the detected cantilever motion itself. In the latter case, the frequency of the cantilever is detected by a frequency counter [42]. Measurements in this section and in chapter 7 are obtained by using a phase locked loop (PLL).

The frequency noise of a cantilever setup is given by two contributing factors, which are the thermal frequency noise and the noise due to the detector.

Thermal frequency noise This noise originates from the power spectral density (PSD) of the thermal force noise on the cantilever, which is given by Eq. 2.9. This force noise is assumed to be constant over the frequency range relevant for each mode of the cantilever. The power spectral density of the stiffness shift (change in spring constant) is dependent on the spectral force noise and the cantilever driving amplitude (A) [43, 42]:

$$S_k = \frac{S_F}{A^2} \tag{3.5}$$

The corresponding power spectral density of the thermal frequency noise in units $\mathrm{Hz}^2/\mathrm{Hz}$ can be approximated by:

$$S_f = \frac{S_k f_0^2}{4k_0^2} \qquad S_k \ll k^2 \tag{3.6}$$

Combining Eq. 2.9, Eq. 3.5 and Eq. 3.6, results in:

$$S_{fT} = \frac{f_0 k_B T}{2A^2 \pi Q k_0} \tag{3.7}$$

Typical values that are used in our MRFM experiment are: Temperature $T = 50$ mK, eigenfrequency $f_0 = 3$ kHz, driving amplitude $A = 1$ nm, quality factor $Q = 10000$ and spring constant $k = 8 \cdot 10^{-}5$ N/m. This results in a spectral frequency shift due to thermal force noise $\sqrt{S_{fT}}$ of 0.4 mHz/$\sqrt{\mathrm{Hz}}$.

Detector noise When measuring the movement of the cantilever, noise will be introduced by the sensor detecting the motion, which can be a combination of several noise sources. In the case of our MRFM setup, the major noise is originating from the SQUID. The SQUID-noise is partly generated by shunt resistors [44, p. 37-42] and is composed of white noise with a 1/f component. Usually, the frequency of the cantilever is high enough to discard the 1/f component. The power spectral density of the detector noise (S_{xdet}) can be transformed to a force power spectral density $S_F(f)$ as if it would have been generated by the cantilever:

$$S_F(f) = \frac{S_{xdet}}{|H(f)|^2} \tag{3.8}$$

Where $H(f)$ is the transfer function of the cantilever:

$$H(f) = \frac{1}{1-(f/f_0)^2 + if/(f_0 Q)} \frac{1}{k} \tag{3.9}$$

Since the transfer function (Eq. 3.9) is a peaked function, the spectral function of the effective force noise (Eq. 3.8) increases rapidly when moving away from the resonance frequency of the resonator. Using Eq. 3.5 and 3.6, the frequency power spectral density becomes [43]:

$$S_f(f) = \frac{S_{xdet} f_0^2}{4A^2} \left(\left(1 - \frac{f^2}{f_0^2}\right)^2 + \frac{f^2}{f_0^2 Q^2} \right) \tag{3.10}$$

Noise with PLL The phase locked loop corrects the driving frequency of the cantilever using a PID feedback system in which the phase is used as setpoint. Within the bandwidth of the PID system and the PLL, the output of the PLL is frequency-modulated equal to the frequency noise present at [45, p. 20-26]:

$$f = f_0 \pm f_m \tag{3.11}$$

Where f_m is the modulation frequency. Then, combining the detector noise PSD Eq. 3.10 and the thermal frequency noise PSD Eq. 3.7, we find for the total frequency noise power spectral density for small modulation frequencies ($f_m \ll f_0$) [42]:

$$S_f = \frac{f_0 k_B T}{A^2 \pi Q k_0} + \frac{2 S_{xdet}}{A^2} \left(f_m^2 + \frac{f_0^2}{4Q^2} \right) \tag{3.12}$$

A factor 2 is introduced in this equation since the modulation is two sided around the eigenfrequency of the cantilever.

In figure 3.1, the spectral density of the frequency noise as a function of modulation frequency for different driving amplitudes (by piezo-electric driving) is shown. The measurement is performed by using the setup as described in chapter 2. The center of the magnetic particle on the cantilever is positioned above the copper at a distance of 4.5 μm. Eddy currents are present at this distance, which cause the quality factor of the cantilever to drop ($Q = 1767$ at this distance), which will be discussed in chapter 7. The amplitude, as shown in the legend of the graph, is measured by the output of

the SQUID using a lock-in amplifier. This output is proportional to the displacement of the cantilever. From Eq. 3.12 we see that properties of the cantilever can be found. This may be a useful way to compare parameters such as cantilever temperature and detector noise. In 3.1 is fitted by equation 3.12, in which all parameters are known.

The movement of the cantilever is calibrated to the SQUID output voltage (Vsq) by using the equipartition theorem (far from the surface, where Q = 30000) at 500 mK, yielding 11 nm/Vsq. The temperature at the copper sample was 50 mK, but we observed a saturation of the thermodynamic mode temperature of the cantilever at 139 mK. The quality factor Q ($Q = 1767$) was measured by Lorentzian-fitting the response of the cantilever movement to a piezoelectric actuation which is frequency swept around the eigenfrequency of the cantilever. According to the calibration, the detector noise would be 55 pm/$\sqrt{\text{Hz}}$ (corresponding to $5 \cdot 10^{-6}$ V/$\sqrt{\text{Hz}}$). Further, it is clearly visible that the 1/f component is present.

The origin of this 1/f component is visible in figure 3.2, where the spectral density of the frequency noise at different distances is shown. The quality factor is measured at each distance by Lorentzian fitting. The same parameters as in fig 3.1 were used, with $T = 139$ mK, $A = 110$ nm (at 10 mV detected amplitude) and a detector noise of 55 $pm/\sqrt{Hz}$. It is clearly visible that the 1/f component is dependent on the distance to the sample. The 1/f component is fitted in proportion to the dissipation (1/Q), with a proportionality factor of 1 Hz$\sqrt{\text{Hz}}$. Therefore probably the eddy currents cause low frequency gradient force fluctuations.

In other experiments on different surfaces, 1/f noise is also present [19]. The origin of these fluctuations is not yet completely understood.

3.3 Comparison of a force measurement and a frequency measurement

Different ways of detecting spins in a sample may result in different signal to noise ratios. In this section, we hope to give some clarity in the signal to noise ratio (SNR) and requirements for a force detection on the one hand and a frequency measurement on the other hand.

Signal to noise ratio for a force measurement and frequency shift measurement The frequency shift Δf is proportional to the stiffness shift Δk of the cantilever for small spring constant changes:

$$\Delta f = f_0 \frac{\Delta k}{k_0} \qquad \Delta k \ll k_0 \tag{3.13}$$

Therefore, using Eqs. 2.9, 3.5, and 2.3, the signal to noise ratio of a frequency shift measurement is equal to:

$$SNR_{\Delta f} = \Delta k / k_{noise} \tag{3.14}$$

$$= \mu \frac{\partial^2 B}{\partial x^2} \frac{A}{4 k_B T \Gamma} \tag{3.15}$$

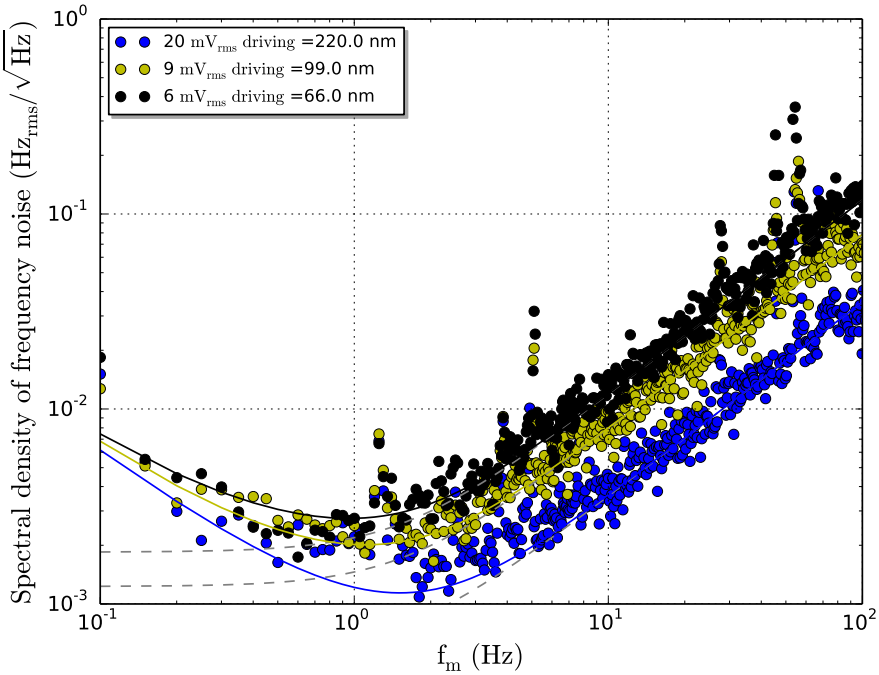

Figure 3.1: Power spectral density of the frequency noise as a function of modulation frequency for different amplitudes of an MRFM cantilever above a copper sample. Cantilever parameters: eigenfrequency $f_0 = 3000\,\mathrm{Hz}$, spring constant $k_0 = 8 \cdot 10^{-5}\,\mathrm{N/m}$, Quality factor $Q = 1767$ and thermodynamic mode temperature $T = 139\,\mathrm{mK}$. The data are fitted with Eq. 3.12. The amplitude of the cantilever motion is measured by a lock-in amplifier. The measured voltage and motion in nm is shown in the legend (with calibration 11 nm/ 1 $\mathrm{mV_{rms}}$). The detector noise is measured to be 5 $\mu\mathrm{V}/\sqrt{\mathrm{Hz}}$, corresponding to 55 $\mathrm{pm}/\sqrt{\mathrm{Hz}}$. The 1/f component is fitted with a factor $a/Q = 0.6 \cdot 10^{-3}\,\mathrm{Hz}\sqrt{\mathrm{Hz}}$, with $a = 1\,\mathrm{Hz}\sqrt{\mathrm{Hz}}$. The segmented gray lines represent the fits without the added $1/f$ noise component.

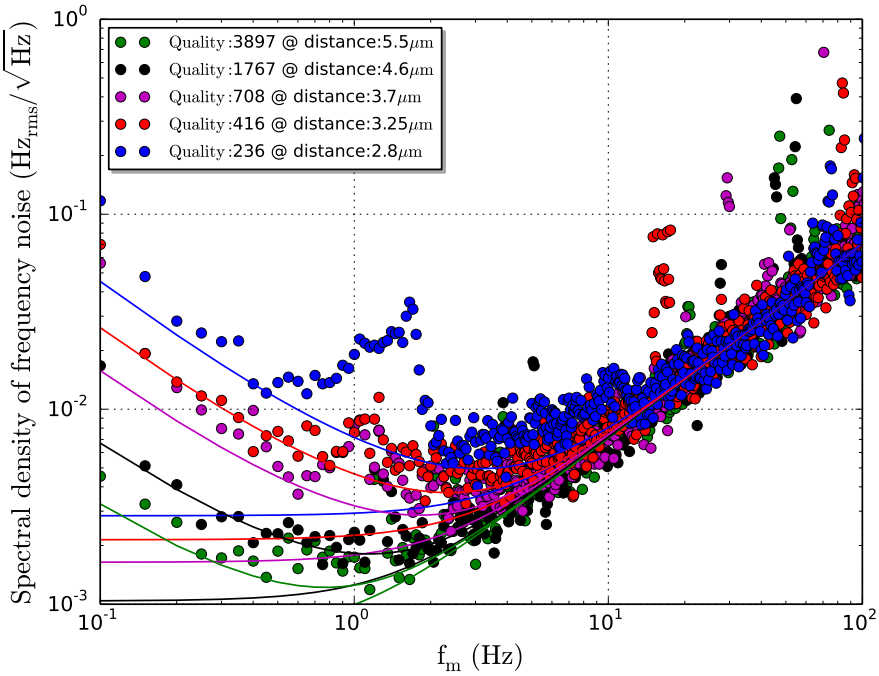

Figure 3.2: Power spectral density of the frequency noise as a function of modulation frequency for different distances of an MRFM cantilever above a copper sample at a temperature of $T = 139\,\mathrm{mK}$. At each height, the piezo-driving amplitude was set to a value such that the measured SQUID voltage was 10 mV (corresponding to a cantilever amplitude of 110 nm). The quality factor was measured by Lorentzian fitting. The cantilever parameters are the same as in figure 3.1, except that the quality factor changes with height. Likewise, the fitting parameters (amplitude = 110 nm at 10 mV and detector noise of 55 $\mathrm{pm}/\sqrt{\mathrm{Hz}}$) are the same. The $1/f$ noise is fitted with the function $\sqrt{S_{1/f}} = \frac{a}{Qf}$ with $a = 1\,\mathrm{Hz}\sqrt{\mathrm{Hz}}$

Where A is the amplitude of the cantilever motion.
The signal to noise ratio of a force measurement is given by:

$$SNR_F = \Delta F / F_{noise} \tag{3.16}$$

$$= \mu \frac{\partial B}{\partial x} \frac{1}{4k_B T \Gamma} \tag{3.17}$$

Using these two signal to noise ratios, we can compare the signal to noise ratios of the frequency measurement and force measurement:

$$\text{Improvement} = \frac{SNR_F}{SNR_{\Delta f}} \tag{3.18}$$

$$= \frac{\frac{\partial B}{\partial x}}{\frac{\partial^2 B}{\partial x^2} A} \tag{3.19}$$

$$\propto \frac{d_m}{A} \tag{3.20}$$

Where d_m is the distance to the center of the magnet. For the last proportionality, we assumed a dipole magnet, which has a magnetic field proportional to the inverse cube of the distance.

From this equation, we see that it is favorable in terms of sensitivity to use the force sensing measurement when the distance is larger than the driving amplitude, which is normally the case. In our experiments, we avoid using amplitudes larger than 10 nm and our magnet is typically 4 μm in diameter. Unfortunately, a force measurement requires a larger B_1 field to manipulate spins quickly enough (see chapter 8).

3.4 T_1 requirements of spins

The spin lattice relaxation time (T_1) sets the time in which the spin returns to its equilibrium value with lowest energy, limiting the detection bandwidth. Therefore, the signal to noise ratio of an MRFM measurement may also depend on the relaxation time of the spins. For saturation experiments in which the frequency shift is measured, a large bandwidth is required when materials with short T_1 times are investigated. As visible in figure 3.1, the noise increases at higher modulation frequencies. Although more averages can be applied for shorter T_1, this reduces the noise only by the square root of the number of measurements. The signal may also be masked by spurious cross-talk signals, appearing during B_1 pulses. The recovery time of the signal may then take longer than the relaxation time of the spins. In the case of the experiment on copper as described in chapter 7, relaxation times below 100 ms would be very challenging to measure. On the other hand, when the relaxation time is very long (more than 100 sec), 1/f noise and the required patience may be limiting.

3.5 RF wire: dissipation

In chapter 8 we discuss adiabatic rapid passage, which is a method to flip a spin in an efficient way in inhomogeneous B_1 fields. In order to apply adiabatic rapid passage to

nuclear spins, sufficient radio frequent oscillating magnetic fields (B_1 fields) need to be generated. These need to be in the order of 4 mT, because the adiabatic condition has to be fulfilled, see chapter 8:

$$\frac{(\gamma B_1)^2}{\omega_a A} \gg 1 \tag{3.21}$$

Where $\omega_a = 2\pi/T_p$ is the angular pulse frequency, with T_p the pulse length, A is the modulation frequency amplitude around the larmor frequency and γ is the gyromagnetic ratio. For cyclic adiabatic cantilever driving, usually the angular pulse frequency equals two times the angular eigenfrequency ω_0 of the cantilever ($\omega_a = 2\omega_0$).

The difficulty with MRFM at millikelvin temperatures is to generate these B_1 fields (or RF fields) while minimizing the dissipation by the RF source, because cooling powers at very low temperatures (10 mK) are limited to approximately 1 μW at the mixing chamber and to even smaller values at the sample. By using a micro wire with high current-densities, one can minimize the dissipation. As a reference, the use of a copper micro wire to produce a B_1 field of 4 mT (M. Poggio et. al.) results in 350 μW power dissipation at 300 mK temperature at the mixing chamber of a dilution refrigerator [30]. The temperature at the sample is likely to be higher, since the RF-source is located closer to the sample than to the mixing chamber.

In order to even further lower the dissipation, we used a superconducting RF micro wire. The design of the micro wire together with sample and detection circuit is shown in figures 2.6 and 2.9. We used niobium titanium nitride (NbTiN) as superconducting material, since this material is known to have a large bandgap and very low dissipation at high frequencies in the sub-mm range [46]. We studied the dissipation mechanisms for alternating currents in a NbTiN superconductor. A detailed explanation of the experiments and the dissipation mechanisms is described in the Master thesis of K.M. Bastiaans [31]. In this study, a similar sample as shown in figure 2.9 was used, in which the critical current of the RF wire was measured to be 18 mA. Consequently, using the Biot-Savart-law, a constant magnetic field of 4 mT at 1 μm distance can be generated. Despite the large DC current and constant magnetic fields, the dissipation turned out to be significant already at 100 kHz and increasing at higher frequencies. The dissipation as well at low temperatures (10-100 mK) as at higher temperatures (4K) showed a quadratic behavior as a function of frequency. Similarly, a quadratic dissipative behavior was seen as a function of current.
Three possible reasons for this dissipation mechanism were proposed; dissipation through quasiparticles, vortex dynamics, and dilectric losses in the substrate [31, p. 9-19]. Using the Usadel equations, an estimate of the quasiparticle density of states could be made at different temperatures for the NbTiN micro wire. This shows, despite a quadratic frequency behavior, that no (or negligable) quasiparticles are formed at 10-100 mK temperatures. The dissipation due to dielectric losses would show a linear frequency dependence, leaving dissipation through vortex dynamics. For large current densities, the Lorentz-force for vortices may be larger than the pinning force of the vortices, causing movement (depinning) of vortices. As a consequence, a dissipation channel is created. Another dissipation channel could be created by vortex oscillations in the potential well of a pinning site due to the oscillating current. In contrast with a quadratic behavior of the former, the latter shows a linear dissipa-

tion as a function of frequency. Therefore, in conclusion, the most feasible dominant dissipation channel in this superconductor (NbTiN) is the depinning of vortices [31, p. 37]. The measurements show that a dissipation of 150 nW is generated at a current of 2 mA at a frequency of 100 kHz.

3.6 NbTiN RF wire: reduced repulsion

The RF wire and the pick-up coil are superconducting. Due to the Meissner effect, supercurrents which counteract the magnetic field from the magnetic particle, are created. As a result, the magnetic particle on the cantilever is repelled. However, in a superconductor, the magnetic field can only penetrate until a certain depth, called the penetration depth. This repelling force decreases for larger penetration depths, especially if the size of the superconducting structures approaches this depth. This is the case for the superconducting NbTiN pick-up coil and RF wire as shown in figure 2.9. The wire dimensions are 0.3 μm x 2 μm for the RF wire and 0.3 μm x 1 μm for the pick-up coil, while the penetration depth for the NbTiN film is measured to be 280-300 nm and. Because of this large penetration depth (also called London penetration depth), we would expect less repulsion from the NbTiN superconductor.

To show this experimentally, the frequency shift at 8.5 μm $\pm$ 0.5 μm distance from the surface as a function of x position above the pick-up coil is shown in figure 3.3. In addition, a simulation, assuming no penetration depth, is shown in the same figure. This simulation is also used in the thesis of G. Wijts, in which it fits the data of a magnetic particle above a niobium superconductor well [26, p. 49-56]. The position path is shown in the inset of the figure.

We indeed see that the repulsion above the NbTiN superconductor is significantly less (more than a factor four) than in a type I superconductor with small penetration depths. The uncertainty in the simulation, represented by solid gray lines from the upper and lower limit in figure 3.3, is due to the uncertainty in film-thickness. This thickness has been influenced by the etching procedure, where after observing a short in the circuit an extra over-etching time corresponding to 20% of the total RIE etch time was set. The film thickness before etching was 378 nm, which would be reduced to 300 nm with 20% over-etch time. A possible further reduction in size may be present from a faster etching speed of small, micrometer structures. Therefore to be in a safe limit, the gray lines in figure 3.3 restrict the thickness between 150 nm and 350 nm. The blue line corresponds to 250 nm thickness. In future, the thickness could be measured by atomic force microscopy (AFM). One also has to take care that at small distances between the superconducting wire and the magnetic particle, the first critical field at 8mT for NbTiN is passed, allowing vortices to enter, which complicates the interpretation. These vortices may also lower the quality factor of the cantilever. This is not an issue for the measurements shown in figure 3.3, because the magnetic field from the magnetic particle at 8.5 μm distance is 3-5 mT.

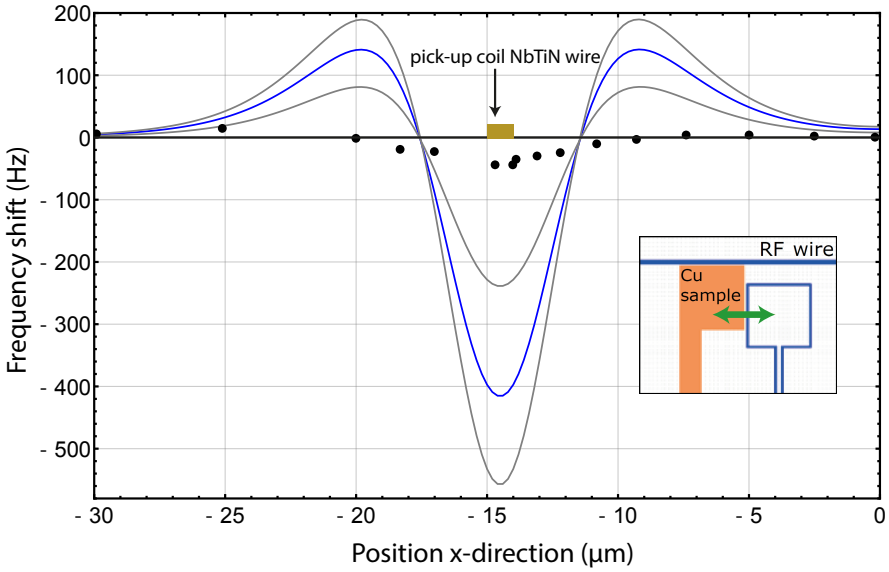

Figure 3.3: Repulsion of the magnetic particle on the cantilever due to the superconducting pick-up coil wire at a distance of 8.5 μm $\pm$ 0.5 μm. The black dots represent the data and the blue and gray curves represent the simulation. We find that the repulsion is at least four times lower than a calculation which indicates that the large London penetration depth of NbTiN $\lambda = 280 - 300$ nm significantly reduces the magnet. The gray lines form an upper and lower bound for the simulated repulsion, calculated with two different film thicknesses (150 nm and 350 nm). This uncertainty in film thickness is due to the etching procedure. The blue line represents the intermediate simulation, which corresponds to 250 nm thickness.